REPORT DOCUMENTATION PAGE

Form Approved

OMB No. 0704-0188

1. REPORT DATE *(DD-MM-YYYY)*	2. REPORT TYPE	3. DATES COVERED *(From - To)*
11-08-2015	Final	28 Mar 13 to 27 Mar 15

4. TITLE AND SUBTITLE

Radar Control | Optimal Resource Allocation

5a. CONTRACT NUMBER
FA2386-13-1-4080

5b. GRANT NUMBER
Grant AOARD-134080

5c. PROGRAM ELEMENT NUMBER
61102F

6. AUTHOR(S)

Prof. William Moran

5d. PROJECT NUMBER

5e. TASK NUMBER

5f. WORK UNIT NUMBER

7. PERFORMING ORGANIZATION NAME(S) AND ADDRESS(ES)
Univ of Melbourne
Grattan St,
Parkville. VIC 3010
Australia

8. PERFORMING ORGANIZATION REPORT NUMBER

N/A

9. SPONSORING/MONITORING AGENCY NAME(S) AND ADDRESS(ES)

AOARD
UNIT 45002
APO AP 96338-5002

10. SPONSOR/MONITOR'S ACRONYM(S)

AFRL/AFOSR/IOA(AOARD)

11. SPONSOR/MONITOR'S REPORT NUMBER(S)
AOARD-134080

12. DISTRIBUTION/AVAILABILITY STATEMENT

Distribution A: Approved for public release. Distribution is unlimited

13. SUPPLEMENTARY NOTES

14. ABSTRACT
This proposal will work towards the eventual realization of a long term goal of developing, waveforms and other radar resources, scheduling of those resources, and the processing of target returns to provide high performance detection and tracking using resource agility for a realizable radar system.

15. SUBJECT TERMS

Radar Systems, Radar Resource Scheduling, Golay Codes, Doppler Resilient Processing, Cognitive Radar

16. SECURITY CLASSIFICATION OF:			17. LIMITATION OF ABSTRACT	18. NUMBER OF PAGES	19a. NAME OF RESPONSIBLE PERSON
a. REPORT	b. ABSTRACT	c. THIS PAGE			Seng Hong, Ph.D.
U	U	U	SAR	30	**19b. TELEPHONE NUMBER** *(Include area code)* +81 4 2511 2005

Standard Form 298 (Rev. 8/98)
Prescribed by ANSI Std. Z39.18

AOARD Project Report

Final technical report for the project period March 2013 – May 2015 under Grant No. FA2386-13-1-4080

Professor Bill Moran

July 13, 2015

Contents

1 Overview

Project title: Radar Control — Optimal Resource Allocation

This report addresses several issues arising in discussions with Braham Himed as well as our work to date.

The key components are:

1. Track before detect techniques: This arose in a discussion with Braham Himed. The description given here is for information only. It is a technique we have implemented several times in the past, alongside other innovations, as have several other researchers. This part of the document has been presented in previous reports to AFRL as part of a Prometheus contract.

2. Mode scheduling: again this is a presentation of earlier work by the group, also reported under a Prometheus contract, and again in response to a request by Braham Himed.

3. Opportunistic bandwidth radar: this is new work aimed at attempting to understand scheduling in a time-dependent bandwidth limited situation. The idea is to choose pieces of bandwidth as and when they become available.

4. Clutter modelling for detection: this represents part of our work on the contract. A component of waveform and other resource scheduling requires clutter to be modelled, in real time. Here is presented a simple approach that appears to perform better than some existing techniques.

5. Information gain from radar scheduling: this is an early attempt to understand how to compare gain in a radar from measuring immediately rather than waiting to choose a better waveform. While this work is preliminary it suggests that it is not always better to schedule resources for gain of information.

6. More simulation based studies were carried out and results are reported in Section 7.

2 Integrated detection and tracking

Tracking algorithms in radar typically work with a set of "detections" obtained after applying statistical tests to the radar returns in each cell of the surveillance area. The statistical testing procedure involves comparing the matched filter output to a threshold selected to give a specified false alarm probability. This traditional approach does not consider the dependence of tracking performance on threshold selection. This dependence was first considered in [1] where the detection threshold was selected to minimise an approximation to the mean square error. A similar idea was pursued in [2, 3]. All of these methods are based on the sub-optimal probabilistic data association filter (PDAF) [4] and the analysis performed in [1]. The basic idea is as follows. The PDAF provides a Gaussian approximation to the posterior. Let $P_{k|t}$ denote the covariance matrix of this approximation for the state at time k based on measurements up to time t. It was shown in [1] that, averaged over the measurements, the one-step ahead covariance matrix can be approximated as

$$\mathsf{E}[P_{t|t}] \approx P_{t|t-1} - q(\Gamma, S)W_t \tag{1}$$

where $q(\Gamma, S) \in [0, 1]$ is the information reduction factor for a detection threshold Γ and SNR S and W_t is a positive definite matrix. Assuming the SNR S is known, the trace of the expected covariance matrix can be minimised by maximising $q(\Gamma, S)$ as a function of Γ. Although $q(\cdot, S)$ cannot be evaluated in closed-form it was shown in [2] that, for a special case, a function can be fitted to $q(\cdot, S)$ and the optimal value of Γ found in closed-form. Interestingly, the optimal Γ for

tracking purposes usually results in a false alarm probability far in excess of those commonly used in radar signal processing.

A different approach was used in [5] where the available knowledge of the target's position was used to formulate a Bayes detector which increases the detection probability in the vicinity of the estimated target position. This results in a detector with a spatially-varying threshold.

The existing methods described in [1, 2, 3, 5] have a number of limitations:

- All methods are based on the sub-optimal PDAF. It would be of interest to consider the problem of integrated detection and tracking using better alternatives such as particle filters.
- The methods of [1, 2, 3] are based on MSE minimisation. This is not always of interest when tracking in clutter. In such cases, track continuity may be of more interest than tracking accuracy.
- All methods are limited to the case where it is known that only a single target is present. In general, the number of targets cannot be assumed to be known and methods for handling multiple targets are required. Extending existing methods to this case is of great interest.

3 Mode Scheduling and Simulation

This section for the most part is an abbreviated version of old reports, submitted as part of a Prometheus contract, we make no intellectual property claims, but the ideas here appear to be relevant to a discussion between Bill Moran and Braham Himed.

3.1 Mode-Scheduling for Radar

Modern radar system has some specific objectives:

1. detection of all targets in the region being illuminated, i.e surveillance
2. estimation of the position and trajectory of those targets, i.e tracking
3. identification of the targets,
4. assessment of threat posed by each of the targets, etc.

Accomplishing each of those aims depends on the particular mode that the radar system is using. We envisage a radar in which there is some significant control over the radar system at a fast enough rate that it is possible to change its mode of operation on a time scale consistent with objective tasks above. Moreover we assume that these changes will effect the performance of the radar in accomplishing this task. We assume, in order to be specific, that the task is estimation, which might, as in the context of the simulator we have built, be a "track-before-detect" capability and so encompass both Obj-1 and Obj-2. However, we will describe the objective in the language of tracking. We will also assume that the mode being controlled is one or more of any number of radar parameters, such as Waveform, PRI, CPI, Beam shape, Beam direction, Frequency, etc. The problem now becomes a control problem: how to optimally schedule the control parameter so as to maximize a cost function which measures the effectiveness of the radar in accomplishing its task.

Typically, an MoE will have some estimate of the *current* clutter situation as well, at least in a tracking or track-before-detect situation, of the targets. Thus it is possible to simulate the effects of any given control (such as waveform) on the scene and judge its capability according to a cost function. This sets the scene for consideration of the problem as one in control — in fact stochastic control. We note that classical control techniques assume a knowledge of

the state of the system. Here we only have an estimate of the state of the system based on the prior measurements. This estimate is often referred to as the *information state* and can often be considered as a replacement for the state in making a stochastic control problem into a deterministic one. There are results (so-called *separation theorems*) that show that under a wide range of circumstances the information that arises from prior measurements can be condensed down to a "sufficient statistic" that carries all of the information needed from the prior measurements needed by the scheduler in arriving at its optimal schedule.

3.1.1 One-step ahead control

There are many references in the literature to adaptive radar techniques. Almost all of these describe either passive adaptive radar methods (in which the adaptation is done only on receive — in the processing of the return) or active adaptive methods in which the scheduling is done in a *one-step ahead or greedy* way. This method seeks at the next PRI (or whatever the time-scale used) to choose the waveform that is optimal. This may seem to be the obvious thing to do. One-step ahead scheduling will certainly buy more than fixed mode radars but multi-step ahead scheduling will buy more and there are circumstances in which what is paid in computation is worth it.

3.1.2 Closed Loop Scheduling

This is the optimal multi-step scheduling technique. At each step the cost function is evaluated for the next N steps based on the predictions described above. The optimal schedule is selected and implemented *for the next epoch only*, and the process is repeated using the new measurement to enhance the prediction. In this way all information is used at each step of the scheduling algorithm.

As can be imagined, this is computationally very demanding. The calculation of the optimal schedule is a difficult dynamic programming problem and this has to be done at each epoch (so perhaps each PRI) and in order to do this the new measurement has to be incorporated into the estimates and predictions at each epoch.

3.2 Computer Simulations

Under the Prometheus effort we developed a computer GUI that allowed simulation of various tracking scenarios, i.e the number of targets on the scene with various birth/death times, their trajectories, radar cross-sections, etc. Various clutter scenarios are provided, ex. stationary of moving clutter, land or sea clutter and the amount of clutter on the scene could be selected. Waveform (using a small library of waveforms) and beam scheduling algorithms are implemented to allow longer time for performing the surveillance (smart surveillance). The simulated results are shown in the GUI and the statistic of the outcome is computed and shown. An example of such outcome is shown in Figure 1. Here, the three scheduling algorithms are compared, one and two steps ahead scheduling with smart surveillance were tested against the algorithm with surveillance scheduled at regular time intervals.

4 Opportunistic Bandwidth Radar

4.1 Background

In the situation when the whole bandwidth is unavailable, the available smaller bandwidths can be utilized with opportunistic radar. Suppose, that the total bandwidth is 1 GHz, but only 1Mhz of it is available at any time. In this work we assume that available bandwidths are detectable

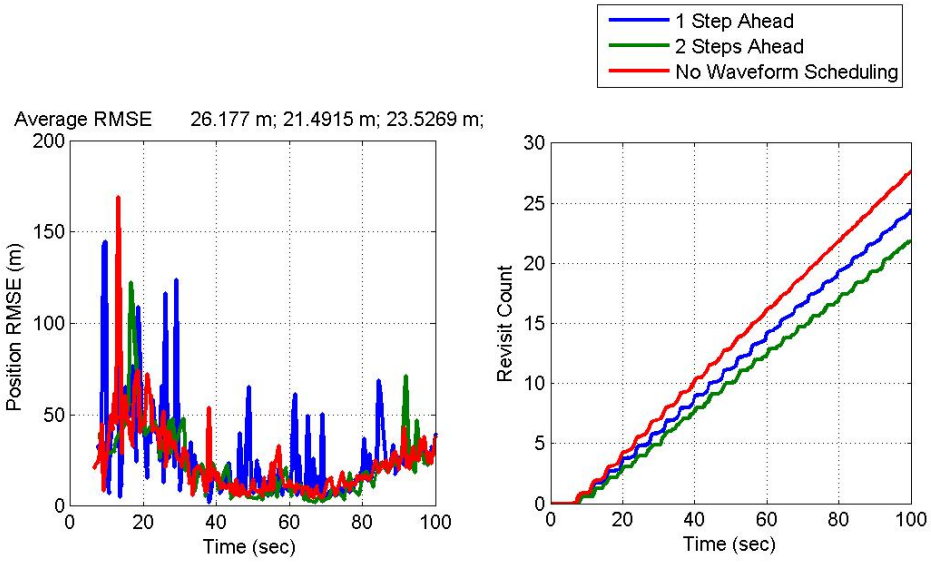

Figure 1: The RMSE and Target Revisit Time with Smart vs. Regular Surveillance

and known, but appear at random frequencies within the total frequency band. Either up-sweep of down-sweep LFM waveform can be transmitted in the available band.

$$s = [\exp(2\pi i \frac{B}{L} t_1^2/2),\ \exp(2\pi i \frac{B}{L} t_2^2/2),\ \ldots, \exp(2\pi i \frac{B}{L} t_n^2/2)], \tag{2}$$

where n is the number of pulses transmitted, B is either 1 GHz or -1GHz total band for up-sweep or down-sweep LFMs, L - total pulse length. $t_1,\ t_2, \ldots, t_n$ are computed as $\frac{L\{f_j, f_j+\Delta f\}}{B}$, where $f_1, \ldots, f_n$ are frequency bands available at time instances $j = 1, \ldots .n$ and $\Delta f = 1$MHz available bandwidth. Square brackets represent vector concatenation, curly brackets represent (frequency) interval. A spectrogram for such transmission is shown in Figure 2. The autocorrelation of such signal is shown in Figure 3. It can be seen that it has good autocorrelation properties. Hence, a stationary scatter could be detected with such a signal. This is not the case for moving scatterer, because the return pulse will have an unknown doppler shift. This is shown in Figure 4.

4.2 Signal processing

It is possible to improve the performance by rearranging the returns. For stationary reflectors, the return signal can be "unscrambled", by sorting $f_1, f_2, \ldots, f_n$ in acceding order and concatenating the returned signals in this order. The auto-correlation of this signal is shown in Figure 5. If the Doppler shift f_d is known, then the above procedure can be performed , after "Doppler compensation", i.e by modulating the return with $\exp(-2\pi i f_d t)$.

We consider the following algorithm.

- Perform standard Doppler processing
- Compensate return signal with Doppler, obtained in previous step
- Unscramble the signal

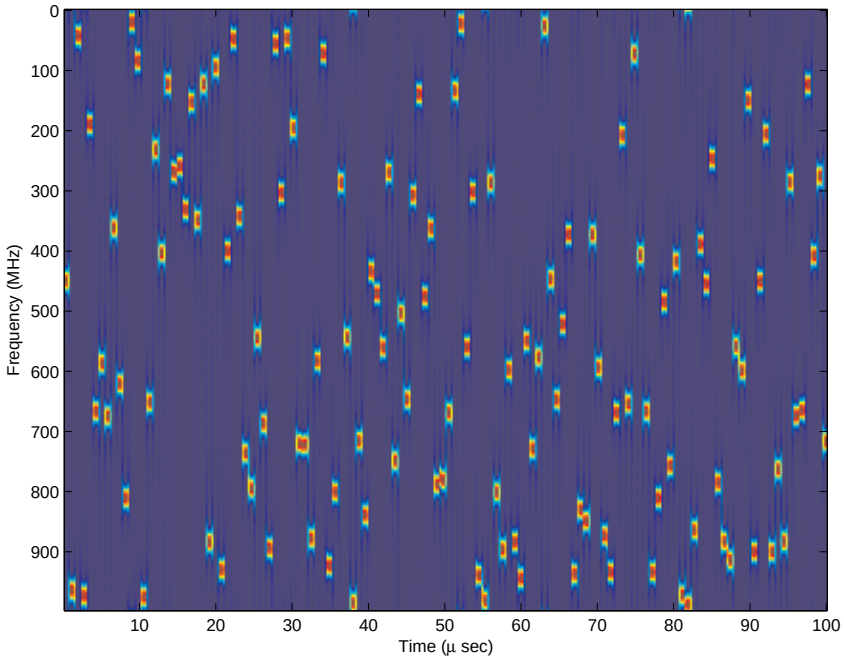

Figure 2: A spectrogram of the waveform transmitted with an opportunistic radar

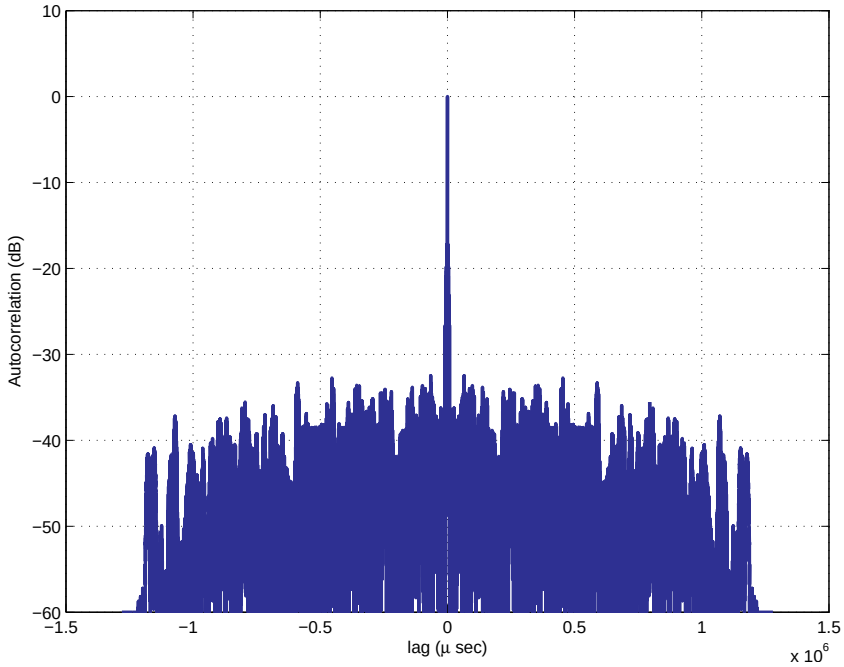

Figure 3: An auto correlation of the waveform transmitted with an opportunistic radar

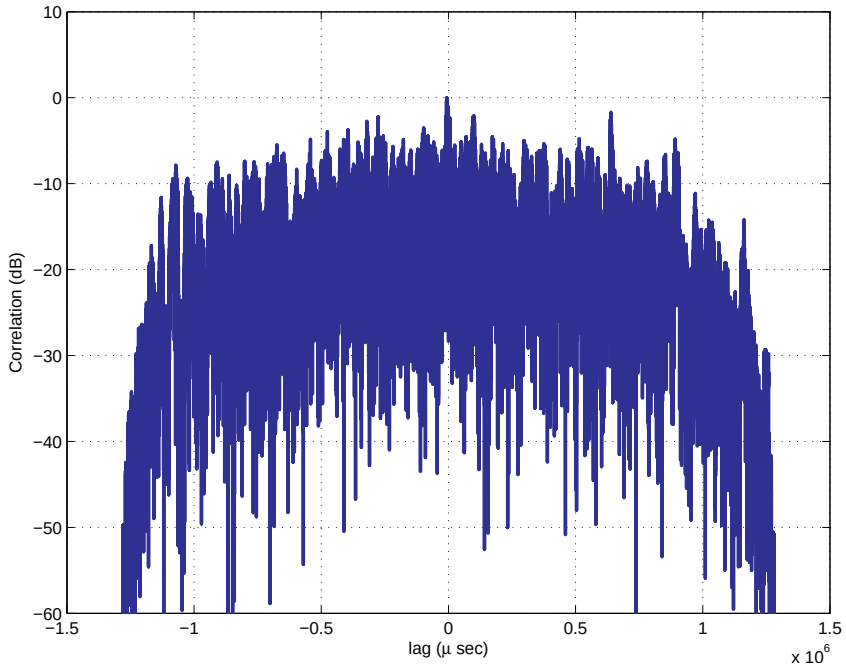

Figure 4: A processed return of the waveform transmitted with an opportunistic radar reflected from a moving scatterer

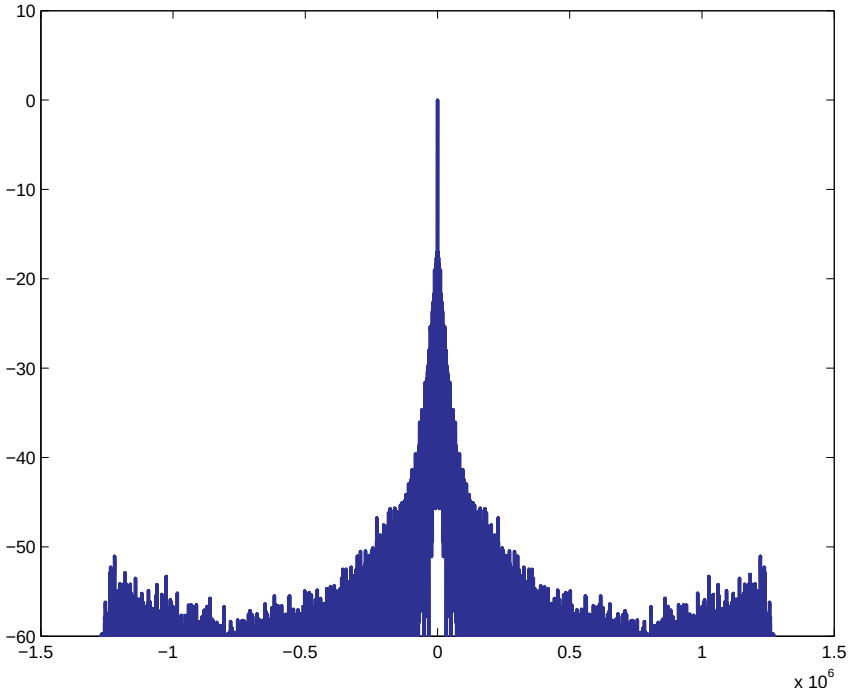

Figure 5: An auto-correlation of the waveform transmitted with an opportunistic radar, unscrambled

- Detect Range
- Use this information to track the targets
- Refine the search from step 1, using the optimum waveform, computed on the tracking step.

The simulation results of the above algorithm is shown in Figure 6. In this example target speed 10.5 m/s. This shows that the proposed method significantly reduces the sidelobes of the return even in the presence of the Doppler shift.

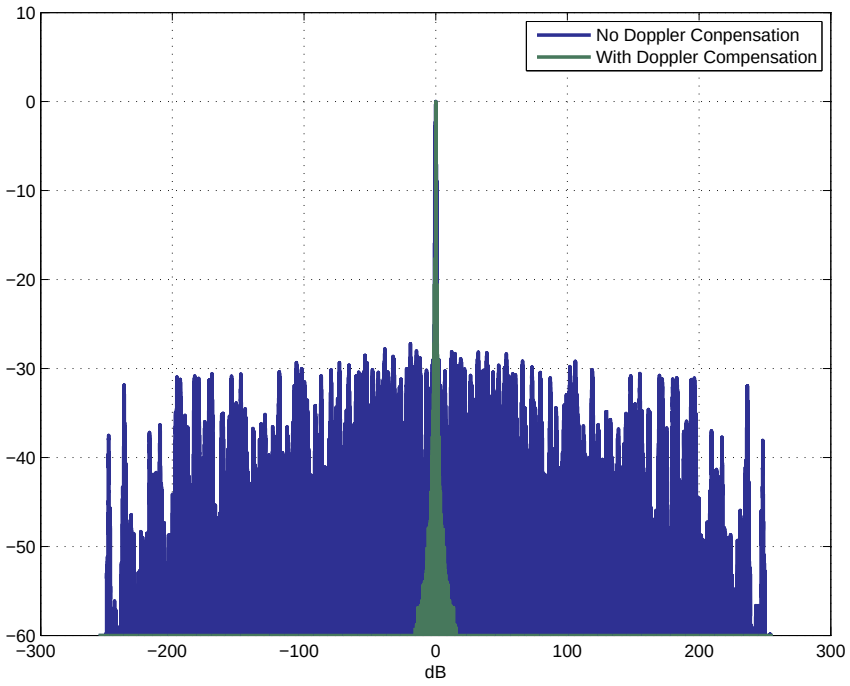

Figure 6: Processed Radar Return with and without Doppler Compensation Method with slow moving target (target speed is 10.5 m/sec)

5 Sea clutter modeling

Sea clutter is the unwanted echoes resultant from radar returns reflected off the ocean surface when operating a radar within a maritime environment. The prevalence of this physical phenomena routinely presents a challenge for the radar designer, frequently presenting itself as the dominant noise component in particular at low-grazing angles. It has the potential to place limitations on the detectability of targets that may be obscured its presence sea clutter due to the physical structure of the sea.

We are interested in developing parsimonious models which exploit the inherent structure of sea clutter. When the sea is considered to be fully developed, sea clutter over a reasonable observation period ($> 30\,\mathrm{s}$) can be observed to possess a quasi-periodic structure for a given patch of ocean. This phenomenon is synonymous with the observed waves present at the ocean surface, with a characteristic periodic structure clearly visible in a radar range-time plot. By assuming that the sea clutter is a cyclostationary process, we estimate a set deterministic components that form the *texture* or macrostructure component of the sea clutter which has been shown to valid model for longer observation periods. Previous statistical estimates of these deterministic components [6, 7] did not consider the spatial relationship of adjacent rangebins in

the measurement set, instead independently estimating the texture for each range bin. Here we seek to derive both the temporal and spatial relationship of the estimated texture components.

5.1 The Compound Gaussian Sea Clutter Model

At any point of the ocean surface, the observed waves are the result of the locally generated wind (capillary) waves (short waves) modulated onto the longer (gravity) waves that may last several days and propagate long distances. This permits the representation of the sea clutter using two different surface roughness scales: one that describe the small scale roughness or *speckle* often associated with whitecaps and foam and the large scale roughness, the *texture* associated with the swell. Then, the complex envelope of the return can be modelled as, for $n = 1, \ldots, N$,

$$z(nT) = \sqrt{\tau_n}\, x_n \tag{3}$$

where T represents the radar pulse-repetition interval (PRI) that is fixed over the interrogation period, $\{\tau_n\}$ is the texture and $\{x_n\}$ is the speckle. Here we further assume that thermal noise is negligible in comparison to the clutter. In the compound Gaussian model, the speckle $\{x_n\}$ is a circular complex white Gaussian process.

The conventional, non-parametric way of estimating the sea clutter is to apply a low pass filter. Let

$$I(nT) = |z(nT)|^2 = \tau_n |x_n|^2 \tag{4}$$

Then, we can estimate the texture non-parametrically using a moving window (MW) filter [8] of length $L + 1$ as

$$\begin{aligned} \hat{\tau}_n &= 1/(L+1) \sum_{m=n-L/2}^{n+L/2} I\,(mT) \\ &\cong \tau_n/(L+1) \sum_{m=n-L/2}^{n+L/2} |x_n|^2 = \tau_n \hat{\sigma}_X^2 \end{aligned} \tag{5}$$

assuming that thermal noise is negligible. In order for the approximation of (5) to be valid, we select L such that $L_X \ll L \ll L_\tau$, where L_X/T and L_τ/T are the speckle and texture correlation periods, respectively For X-band sea clutter, coherence analysis shows a decorrelation period of about 5 ms to 15 ms for the speckle, whereas the texture decoration times are in the order of several seconds [9, 10].

5.2 Parametric texture estimation

A parametric estimator of texture in the compound Gaussian model (3) can provide a more suitable representation of sea clutter for the purposes of adaptive sensing. The observed periodicity of waves suggests a parameteric texture model of the form [11]:

$$\tau_n\,(\boldsymbol{\theta}_K) = A_0 + \sum_{k=1}^{K} A_k \cos\left(2\pi f_k n T + \phi_k\right) \tag{6}$$

where $\boldsymbol{\theta}_K = \{A, f, \phi\}_0^K$ for the K-th order spectral components of the texture. We further assume that $\{A_k\}_{k=0}^K$ are deterministic positive constants, $\{f_k\}_{k=1}^K \in (0, \omega/2\pi]$ and $\{\phi_k\}_{k=0}^K \in (-\pi, \pi]$.

Previously the model (6) has been considered independently for each range cell. However, in general, we expect that for a fully developed sea, the wavelengths of the cosine components of the swell are similar and the waves travels 'together' in a characteristic periodic behaviour. This spatial relationship can be exploited by assuming the existence of a linear phase relationship in

range between the phases of each frequency component. Consider a texture model that is now the planar sum of a set of harmonics across of a series of contiguous, evenly spaced and sized R range bins.

$$\tau_{n,r}\left(\boldsymbol{\theta}_K\right) = A_0 + \sum_{k=1}^{K} A_k \cos\left(2\pi f_k nT + \phi_k + \psi_k r\right) \tag{7}$$

where now $\boldsymbol{\theta}_K = \{A, f, \phi, \psi\}_0^K$ are the common harmonic components of the texture across all of the range cells and $\{\psi_k\}_{k=0}^K \in (-\pi, \pi]$ is used to describe the phase shift of the k-th harmonic of the texture in range. This variable is expected to be also be related to the wavelength of the harmonic component itself.

This finally allows us to now describe the sea clutter as a function of both range and time:

$$z_r(nT) = \sqrt{\tau_{n,r}}\, x_{n,r} \tag{8}$$

where $\{x_{n,r}\}$ are independent, zero-mean circular complex Gaussian random variables.

Texture estimation from the measured intensity requires the retrieval of closely spaced harmonic components in the presence of the speckle, a complex multiplicative noise. The closeness of these components prevents us from using traditional spectral analysis methods to estimate the harmonics. Instead we use a modified version of the CM-RELAX algorithm [6] that recursively estimates harmonics of the cyclic mean from the texture intensity. This RELAXation algorithm was originally introduced as an optimisation approach for estimating harmonic parameters in data sequences corrupted by autoregressive (AR) noise [12, 13, 14].

We consider two variants of the CM-RELAX Newton. The first independently estimates the frequency components of each range bin, as in [6]. Since we wish to establish a spatial relationship, the frequency estimates from each range bin are then clustered to determine the spatial frequency. The second method estimates the frequency components for R adjacent range bins simultaneously by the exploiting the spatial-temporal relationship of the sea clutter, as in (7). We refer to the first algorithm as independent CM-RELAX and the second as joint CM-RELAX.

The method we introduce here differs from CM-RELAX in a number of ways. Firstly, we exploit the symmetry of the intensity periodogram when estimating its frequency components through maximisation. The prevents the need for estimate both sides of the periodogram to be separately, significantly reducing the time complexity required for the algorithm to run. Additionally, we use the Newton-Raphson method to find the maximum of the periodogram of the k-th order of the cyclic mean. This numerical method provides a practical means of finding closely spaced frequency components without needing to perform extremely long FFTs. By doing this, we found that it was unnecessary to continuously re-estimate the already estimated frequency components until the texture estimate settled as previously done in CM-RELAX.

5.3 Validation

The sea clutter data used to validate the algorithm was collected at Osbourne Heads Gunnery Range, Dartmouth, Nova Scotia, Canada by the McMaster University Intelligent PIXel (IPIX) X-band Polarimetric Coherent Radar during the OHGR - Dartmouth Campaign as shown in Figure 7. This radar is an experimental frequency agile, high-resolution originally developed for the purpose of iceberg detection research. It features a 8 kW TWT operating at 8.9 GHz to 9.4 GHz. The parabolic dish antenna has a beamwidth of 0.9° with a cross-polarisation isolation of greater than 33 dB.

The radar was located on a cliff overlooking the Atlantic Ocean at a height of 30 m in a staring configuration above mean sea level at an azimuthal bearing of 129.5° over the open ocean.

We selected a measurement performed on the November 11th 1993 at 16:36:25, corresponding to the data file `19931111_163625_starea.cdf`. At the time of collection, the sea was reported

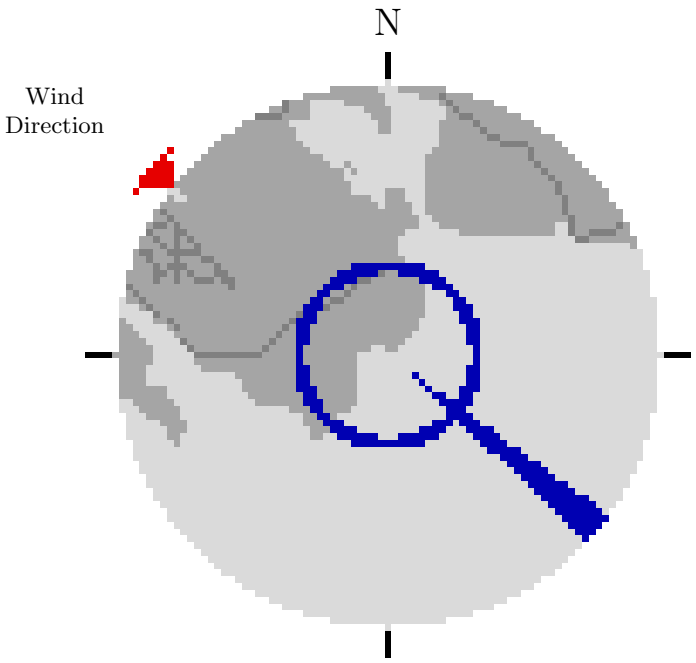

Figure 7: Radar data collection site at OHGR, Nova Scotia. Source:[15]

to having a significant wave height of 0.7 m with a average wave period of 4.4 s. During the measurement period, the radar was operating at 9.39 GHz with a PRF of 1000 Hz with a range resolution 30 m, sampled at 15 m over a period of 131 s. We utilise range bins 1 to 6. This equates to ranges of 2574 m to 2649 m at a resolution of 30 m, sampled at 15 m due to the placement of a target at 2660 m. The results reported here correspond to measurements made in a VV polarisation.

The results shown here apply to the CM-RELAX Newton algorithm being run over a a data set of length 120 s. For the intensity data Y_{k-1} FFT computation, we found that an FFT length of 2^{18} and 2^8 provided sufficient resolution for a good initial peak estimate of ω_k and ϕ_k, respectively. For comparative purposes with the non-parametric MW-Filter texture estimator, we have used a length of 2^{10} samples with equates to a period of 1.024 s.

We first consider the correspondence between the spatio-temporal frequencies obtained by the independent and joint CM-RELAX algorithms. Figure 8 shows the frequencies obtained by independent CM-RELAX for $K = 7$ across the series of six range bins. Five clusters of closely-spaced frequencies are clearly evident. This suggests that the spatio-temporal relationship proposed in (7) has merit. Two of the remaining frequencies were not common across the range bins. This can be attributed to the algorithm not estimating the same frequencies for all range bins.

The phases of the five clustered frequencies are plotted as a function of range in Figure 9(a). The gravity wave phase of the frequency components found by joint CM-RELAX are shown in Figure 9(b). A close correspondence between the slopes of the phases in Figures 9(a) and 9(b) can be seen. This is confirmed in Figure 10 which plots the phase rates, or spatial frequencies, against the temporal frequencies for independent and joint CM-RELAX. The reasonably close agreement between the two algorithms agrees with the notion that the texture that we observe in any range bin is the result of the sea swell that is travelling across the surface of the ocean in range over time, as predicted by (7).

We now consider the prediction performance of the independent and joint CM-RELAX texture estimation algorithms. Performance is measured by the RMS error between the predicted texture estimate and the MW estimate, averaged over time and range bin. The results are shown in Figure 11 for times up to 10 s. The algorithms perform similarly in terms of prediction

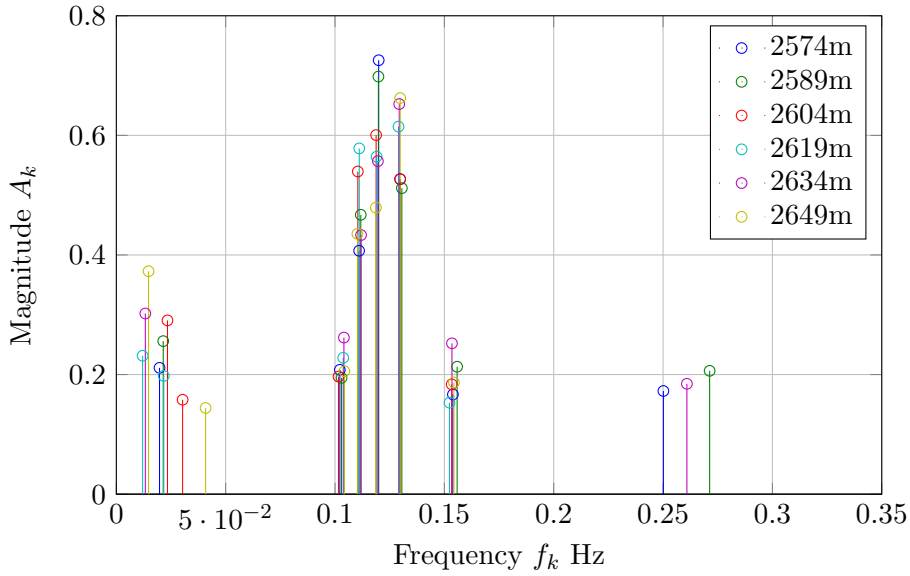

Figure 8: Estimated harmonics $\{\hat{\boldsymbol{\theta}}_K\}$ for $K = 7$

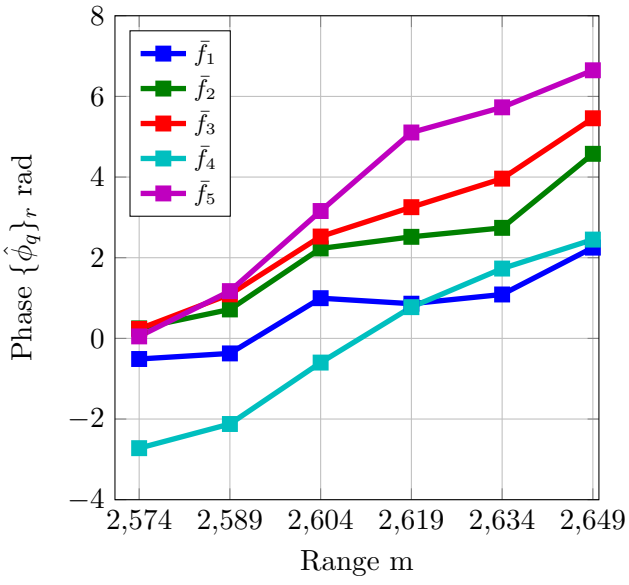

(a) Phase of clustered frequencies for independent CM-RELAX

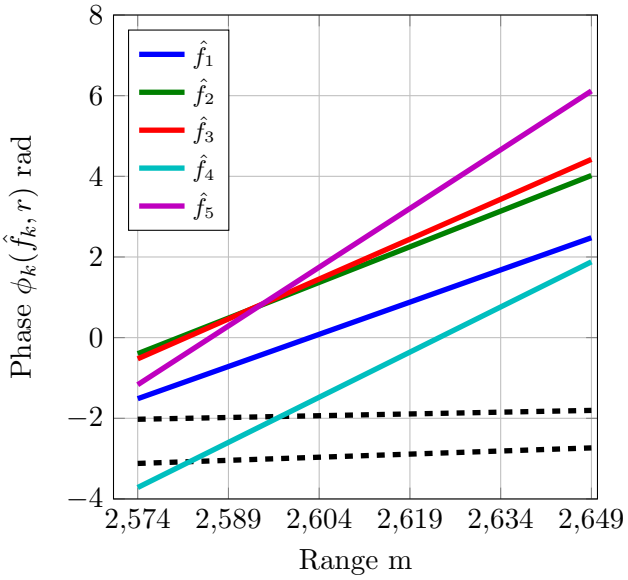

(b) Gravity wave phase for joint CM-RELAX

Figure 9: Clustered harmonic estimates $\{\hat{\boldsymbol{\theta}}_K\}_R$ for $K = 7$

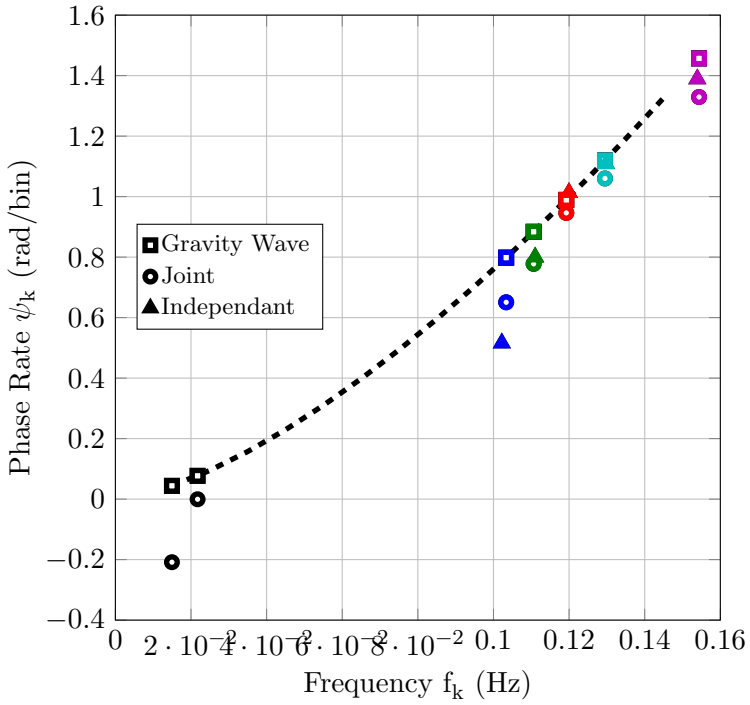

Figure 10: Derived Phase rate $\psi_k\big(\{\hat{\boldsymbol{\theta}}_K\}_R\big)$ compared with jointly estimated phase rate $\hat{\psi}_K$

performance. The RMS error increases rapidly up to 2 s and then remains approximately constant. However, their behaviour as a function of K differs substantially. Joint CM-RELAX performs best for $K = 3$ while independent CM-RELAX favours values of K between 4 and 8 at different times. We attribute this to the ability of the joint CM-RELAX to more easily identify the harmonic components of significance from the intensity data.

5.4 Conclusion

We have developed a compound Gaussian model for sea clutter in which the texture component is modelled by a sum of sinusoids. In contrast to previous work with this model, we considered the spatio-temporal frequency of the texture components. This is motivated by the idea that waves travel across space in a reasonably orderly manner. Comparisons with the usual method of independently estimating frequencies in each range bin using real data demonstrated the validity of our model.

The proposed joint, spatio-temporal sea clutter model has several advantages. First, it allows the sea clutter to be represented by a much smaller number of parameters, therefore resulting in a more parsimonious model which is faster to work with. Second, because inference is performed in 2D frequency space, there is greater separation between the frequency components. As a result the CM-RELAX algorithm performs more reliably. This is manifested in a greatly reduced run time and the achievement of good performance with a smaller number of frequency components. A paper [16] reporting this work has been submitted and is currently under review.

6 Information Gain from Radar Scheduling

6.1 Background

Considerable research effort has gone into the algorithms for scheduling of radar resources; typically, waveforms, but also beam direction and shape and other tunable parameters of radars [17, 18]. Such radar resource scheduling usually demands massive computation. Even myopic

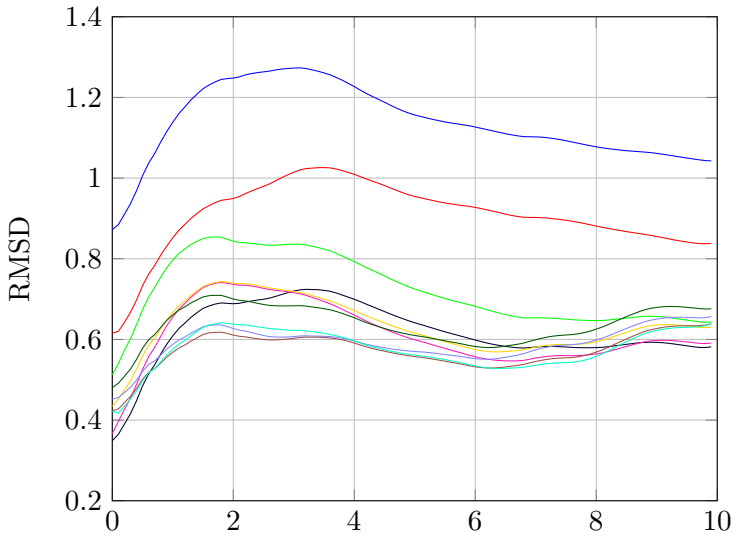

(a) Independent CM-RELAX

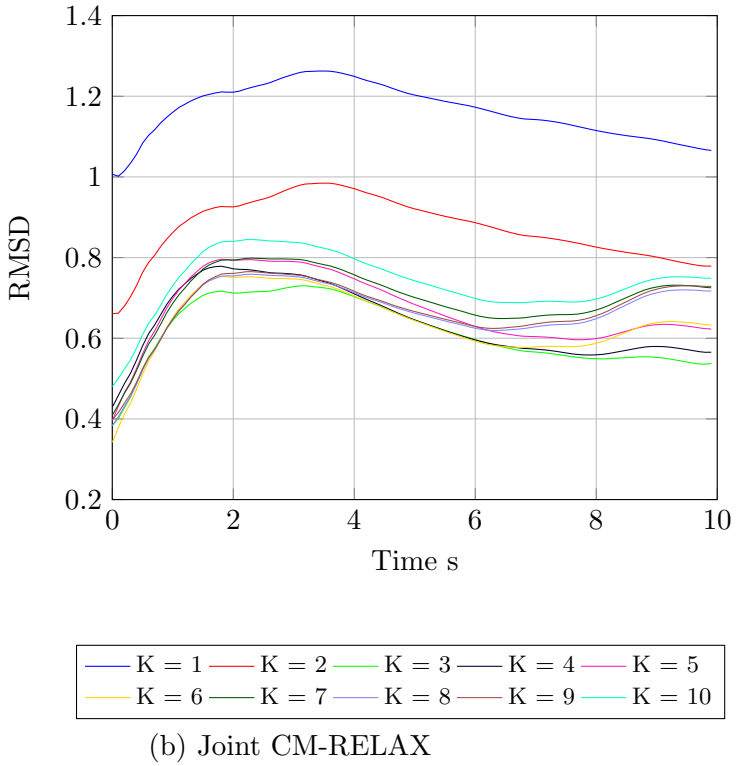

(b) Joint CM-RELAX

Figure 11: RMS prediction error for (a) independent and (b) joint CM-RELAX

scheduling requires evaluation of each feasible value of the tunable parameters against a current representation of the state of knowledge. Even though parsimonious representations of the scene are possible, the computation is non-trivial. When continuous versions of the parameters are used, some kind of gradient descent (or worse still stochastic search) is deployed also requiring many computer clock cycles. Parsimony of representation, while effective in reducing computation also leads to reduced validity of the optimal choice of radar resource. In the non-myopic context, the computational problem becomes exponentially more difficult. Deployment of an optimal scheduling policy over more than just a few radar pulses is computationally infeasible even on normal research timescales, and certainly not at the rate required for real-time deployment in pulse-Doppler radar system, where such computation would require to be completed in at most a few microseconds.

Leaving aside, for a moment, the issue of computer time needed to find the optimal resource, the same kind of issue arises when observing and tracking multiple radar targets. Time spent on a particular target reduces the time available to observe others and to detect new targets. The same kind of issues are at work in this context.

Returning to the computation problem, on the one hand then, a radar system might wait to complete the calculation of an optimal waveform for a particular scene, during which time the target could have significantly changed its state, and on the other choose to use its current best "guess" with the limitations of the use of a "less than optimal" radar resource. This report explores how a radar tracking system can benefit from spending more time in scheduling of radar resources — and thereby achieving better performance — versus using a less than optimal choice of parameters and obtaining more timely information.

We analyze a very simple situation where the measurement quality improves with time spent scheduling the measurement. We consider the situations when measurement error is reduced by scheduling (eg. scheduling waveforms, number of PRI, etc), and when probability of target detection is increased by scheduling (eg. beam scheduling, RM coding, etc). We model target dynamics as Gaussian processes and use the Kalman filter as tracking algorithm. Covariance of target state is used as a measure of improvement. Notice that, in the Gaussian case, this measure is directly related to information gain.

When the state variable is one dimensional the optimal time allocated for scheduling can be computed analytically. While this case is extremely simplistic, it guides our understanding of the more general case. An analytic solution is not available when the state is represented by higher dimensional state variables, but we are able to give a theoretical bound to the time allocated for scheduling.

In this work we assume that the measurement and track processing times are negligible compared to the scheduling time. This assumption is not unreasonable for most modern radar systems. Hence we use the term "scheduling time" to mean "time between measurements".

6.2 One dimensional case, Gaussian model

This very simple case, while unrealistic in practice, gives some insights that are useful for the higher dimensional situation. We assume that the state variable x and the measurement y are scalars (for example: in problem of estimating the range of target)

$$\begin{aligned} \dot{x} &= \text{dynamic noise} \\ y &= x + \text{measurement noise.} \end{aligned} \tag{9}$$

The process is tracked using a Kalman Filter, so that after the nth measurement the state posterior estimate is given by a Gaussian distribution with mean $x_{n|n}$ and variance $\sigma_{n|n}$.

When no measurement is available, the state evolves as

$$\begin{aligned} x_{n+1|n} &= x_{n|n}, \\ \sigma_{n+1|n} &= \sigma_{n|n} + qt, \end{aligned} \tag{10}$$

where t is time and q is a dynamic noise variance for unit time. That is, our uncertainty about the process is assumed to increase linearly over time.

We define radar regime as operating in a "no scheduling" mode when the measurements are taken at the regular time interval $t = 1$ epoch. Now let t be the spent scheduling before the next measurement y_{n+1} is taken.

6.2.1 Measurement accuracy is improved by scheduling

Radar range variance relates to measurement SNR [19] as $r = r_0 + \frac{\Delta x^2}{2\mathrm{SNR}}$, where r_0 is a fixed error variance (due to radar receiver noise and propagation conditions) and Δx is a size of range resolution cell. Consider an example when SNR depends of scheduling time as ct, for some positive c, then

$$r = r_0 + \frac{\Delta x^2}{2ct}. \tag{11}$$

Notice, that c is SNR at time $t = 1$ (i.e in 'no scheduling" mode).

For this and similar examples, we want to write this expression in more abstract terms as $r = a + b/t$, where a, b are real positive constants.

The posterior state variance is computed by Kalman filter as

$$\sigma_{n+1|n+1} = \frac{(\sigma_{n|n} + qt)(b/t + a)}{b/t + a + \sigma_{n|n} + qt} \tag{12}$$

We are interested in finding the scheduling time $t > 1$ which minimizes $\sigma_{n+1|n+1}$. Lets assume that the tracking system is stable, i.e is does not diverge in the "no scheduling" mode. The steady state variance σ in this case is

$$\sigma = \sqrt{q(4a + 4b + q)}/2 - q/2. \tag{13}$$

σ is a lowest possible state variance in "no scheduling" mode, therefore it is appropriate to allow $\sigma_{n|n} = \sigma$. The question is, at what time $t > 1$ posterior state variance surpasses σ. Simplification shows that $\sigma_{n+1|n+1}$ is a rational function of t

$$\sigma_{n+1|n+1} = \frac{\sigma b + (a\sigma + bq)t + aqt^2}{b + (a + \sigma)t + qt^2}. \tag{14}$$

Denoting numerator by $A(t)$ and denominator by $B(t)$, we observe that in the domain of interest (i.e for $t > 1$) both polynomials are positive, hence $\sigma_{n+1|n+1}$ has no zeros or poles. The derivative of $\sigma_{n+1|n+1}$ is proportional to

$$\frac{d\sigma_{n+1|n+1}}{dt} \propto A'(t)B(t) - B'(t)A(t) = q(a^2 - bq)t^2 + 2bq(a - \sigma)t + b(-\sigma^2 + bq). \tag{15}$$

It now can be shown, that for $t > 1$

- If $a > \sqrt{bq}$, then $\frac{d\sigma_{n+1|n+1}}{dt}$ is positive, hence $\sigma_{n+1|n+1}$ is increasing, therefore *we lose accuracy by scheduling.*
- If $a = \sqrt{bq}$, then $\frac{d\sigma_{n+1|n+1}}{dt} = 0$, hence *we gain nothing by scheduling.*
- If $a < \sqrt{bq}$, then $\frac{d\sigma_{n+1|n+1}}{dt} < 0$, hence $\sigma_{n+1|n+1}(t)$ is a strictly decreasing with t with minimum value a at infinity. Therefore *we improve accuracy by scheduling* and scheduling time is unlimited. Incidentally, in this case $\lim_{t\to\infty} \sigma_{n+1|n+1} = a$.

Obviously, similar argument can be applied to a wide range of r, for instance any decreasing $r(t) < a + b/t$ and $a < \sqrt{bq}$ will will also allow unlimited "scheduling" time. Of course, in practice, the scheduling time will have to be restricted by the target range, target detection, presence of clutter, etc. These would have to be taken into consideration when designing a real radar tracking system.

6.2.2 Probability of detection is improved by scheduling

Now, we will analyze the scenario, when the scheduling improves probability of target detection p_d. The posterior variance is computed as

$$\sigma_{n+1|n+1} = \sigma_{n+1|n}(1 - p_d \frac{\sigma_{n+1|n}}{\sigma_{n+1|n} + r}). \tag{16}$$

Consider an example when r is a constant and $p_d = 1 - \alpha/t$, where $0 < \alpha < 1$.

As before we use steady state variance for "no scheduling" as starting point. In this example is

$$\sigma = \frac{\sqrt{q\ (q + 4\,r - 4\,\alpha\,r)} - q + 2\,\alpha\,q}{2 - 2\,\alpha}. \tag{17}$$

We want to find a scheduling time $t^\star > 1$, which minimizes Equation (16) and provides $\sigma_{n+1|n+1} < \sigma$. The derivative of $\sigma_{n+1|n+1}$ is proportional to

$$\frac{d\sigma_{n+1|n+1}}{dt} \propto q(r^2 + \alpha q(r - \sigma))t^2 - 2\alpha\sigma^2 qt - \alpha\sigma^2(\sigma + r). \tag{18}$$

This is quadratic polynomial with at least one real positive root, hence it has the solution $t^\star$ which is computed as

$$t^\star = \frac{\alpha\,\sigma^2\,q + \sigma\,r\,\sqrt{\alpha\,q\ (\sigma + r + \alpha\,q)}}{\alpha\,q^2\,r - 1\,\alpha\,\sigma\,q^2 + q\,r^2}. \tag{19}$$

We are only interested in $t^\star > 1$ and solving the inequality we obtain the following.

- If $\alpha < 0.5$ and $r < \frac{\alpha q}{(2\alpha-1)^2}$, then $t^\star > 1$, and the highest accuracy is achieved at at $t^\star$.
- If $\alpha \geq 0.5$ and $r \geq \frac{q}{1-\alpha}$, then $t^\star > 1$, and the highest accuracy is achieved at $t^\star$.
- Otherwise - longer scheduling time always results in loss of accuracy.

Examples of the state variance as a function of scheduling time for the two cases are shown in Figures 12 and 13.

6.2.3 Probability of detection is improved by scheduling, another example

Consider another example of the above problem. Lets suppose that at time $t = 1$, $p_d = \alpha < 1$. Lets also suppose that after time T of scheduling the probability of detection is $p_d = 1$. We would like to find an answer to a question: what is maximum value of α for which there will be an improvement in state variance at time T. We have $t = T$

$$\sigma_{T|T} = \frac{(\sigma + Tq)r}{\sigma + r + Tq}, \tag{20}$$

where σ is the steady state variance in 'no scheduling" mode (i.e at $t = 1$)

$$\sigma = \frac{q - 2\alpha q + (q(q + 4\alpha r))^{1/2}}{2\alpha}. \tag{21}$$

The solution is the following

$$\alpha < \frac{\left(2qr - 3Tq^2 + 2Tr^2 - qu - 2ru + 2q^2 + T^2q^2 - 4Tqr + 2T^2qr + Tqu\sqrt{Tq} + 2Tru\sqrt{Tq}\right)}{2(Tq - q + Tr)^2}, \tag{22}$$

where $u = \sqrt{Tq\,(4r + Tq)}$. For example, for $q = 1$, $r = 10$, $T = 10$ the probability of detection in "no scheduling" mode α has to be smaller than 0.3332. For $q = 1$, $r = 10$, $T = 3$ $\alpha < 0.5659$. Results for other values of T are shown in Figure 14.

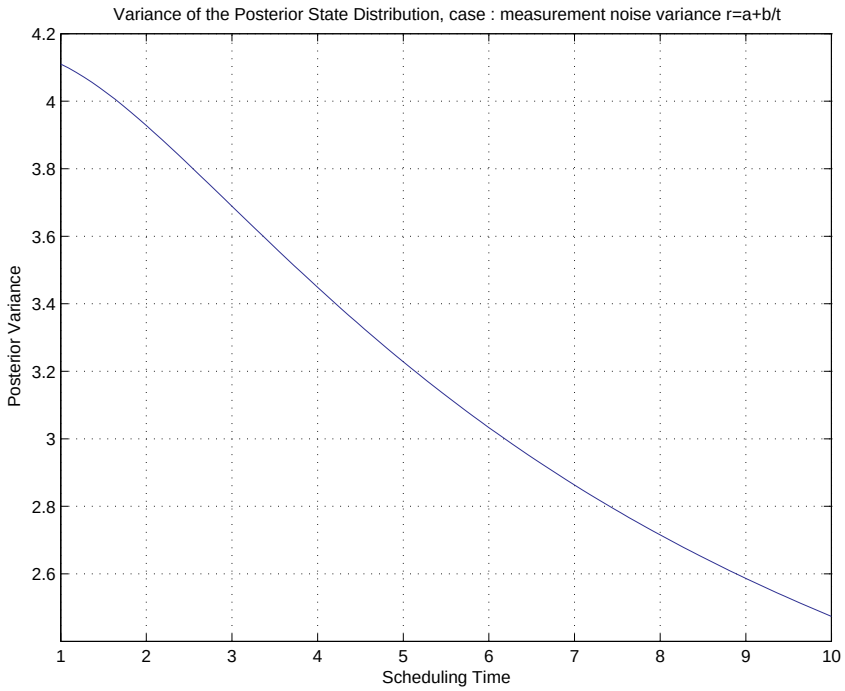

Figure 12: State variance as a function of scheduling time when measurement accuracy is improved by scheduling. In this example $q = 1$, $a = 1$, $b = 10$

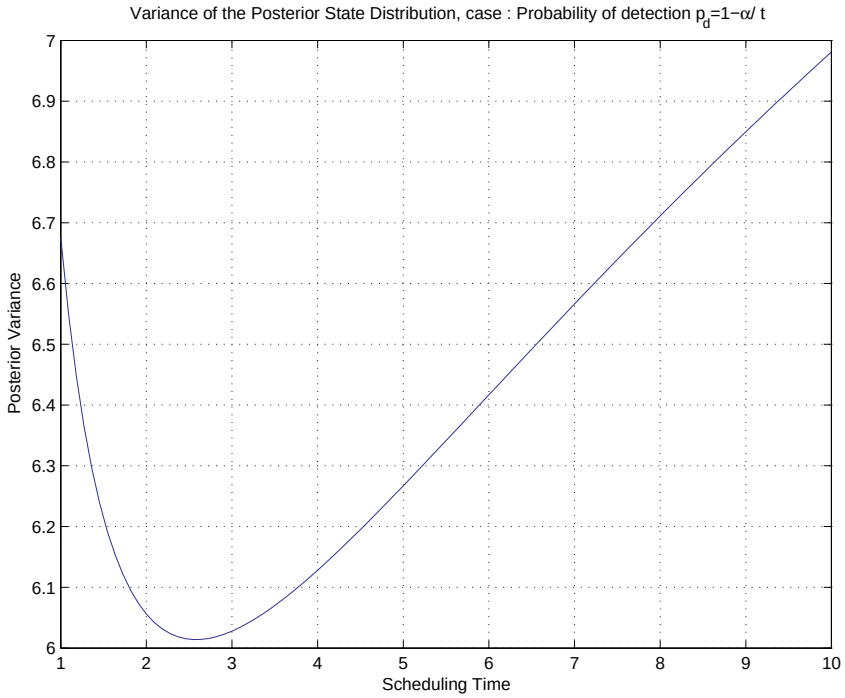

Figure 13: State variance as a function of scheduling time when probability of detection is improved by scheduling. In this example $q = 1$, $\alpha = 0.7, r = 10$

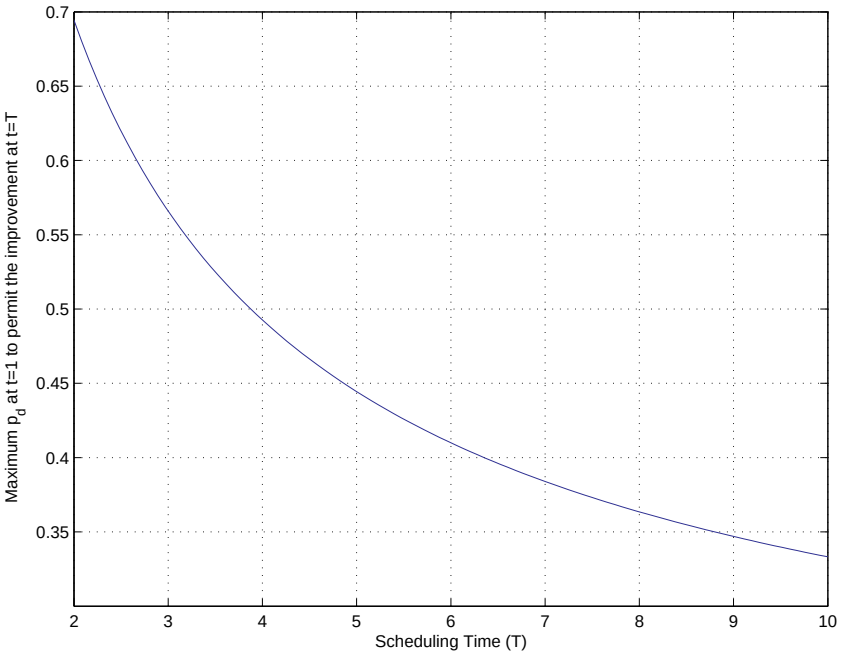

Figure 14: Maximum p_d at $t = 1$ to permit improvement by scheduling at time $t = T$. In this example $q = 1$, $r = 10$

6.3 Two Dimensional Case

Suppose now, that the range and Doppler are measured, the state dynamics and measurements are described as

$$\begin{aligned} \dot{x} &= (I - F)x + \text{dynamic noise} \\ y &= x + \text{measurement noise}, \end{aligned} \tag{23}$$

where I is the identity matrix, $F = \begin{pmatrix} 1 & \tau \\ 0 & 1 \end{pmatrix}$ and τ is time. The dynamic noise is a zero mean Gaussian process with covariance $Q(\tau) = q \begin{pmatrix} \frac{\tau^3}{3} & \frac{\tau^2}{2} \\ \frac{\tau^2}{2} & \tau \end{pmatrix}$, the measurement noise is drawn from a Gaussian pdf with zero mean and covariance R. In the first example we assume that the $p_d = 1$. Let $R(t)$ be a measurement noise covariance matrix which can improve with scheduling time t. Unlike in one dimensional case, the improvement could be achieved in size, shape and orientation of R. The aim is to minimize the determinant of the posterior state covariance matrix as a function of scheduling time. We write

$$\begin{aligned} P_{n+1|n} &= FP_{n|n}F^T + Q(t) \\ \det(P_{n+1|n+1}) &= \det(I - P_{n+1|n}(P_{n+1|n} + R(t))^{-1}) \det(P_{n+1|n}), \end{aligned} \tag{24}$$

where t is the scheduling time. As above it is (almost) equal to the time between nth and $(n + 1)$th measurements.

6.3.1 Measurement Accuracy improves with Scheduling Time

In this example we postulate that scheduling will improve measurement accuracy as $R = R0/t$, then the calculations show, that

$$\det(P_{n+1|n+1}) = |R_0| \frac{A_4(t)}{B_6(t)}, \tag{25}$$

where $A_4(t) = a_0t^4 + a_1t^3 + a_2t^2 + a_3t + a_4$ and $B_6(t) = b_0t^6 + b_1t^5 + b_2t^4 + b_3t^3 + b_4t^2 + b_5t + b_6$ are positive (for $t > 1$) 4th and 6th order polynomials in t, with following coefficients

$$\left[q^2, 4p_{22}q, 12p_{12}q, 12p_{11}q, 12|P|\right] \tag{26}$$

for A_4 and

$$\begin{aligned}\Big[q^2, 4p_{22}q,\ 4q(3\,p_{12} + r_{22}),\ 12(p_{11}q + p_{22}r_{22} - qr_{12}),\\ 12(|P| + 2r_{22}p_{12} - 2p_{22}r_{12} + qr_{11}),\ 12\mathrm{tr}(PR_0^{-1})|R0|,\ 12|R_0|\Big]\end{aligned} \tag{27}$$

for B_6.

$\det(P_{n+1|n+1})$ is positive on the domain of interest ($t > 1$) and it has no zeros or poles in the domain. It behaves like $1/t^2$ for large t. So we conclude that there are no local minima in the domain.

Numerically simulations also show that $\det(P_{n+1|n+1})$ is decreasing with time. In this example $q = 1$, $R = \begin{pmatrix} 5 & 2 \\ 2 & 1 \end{pmatrix}$ It appears that for reasonable values of parameters $\det(P_{n+1|n+1})$ is a

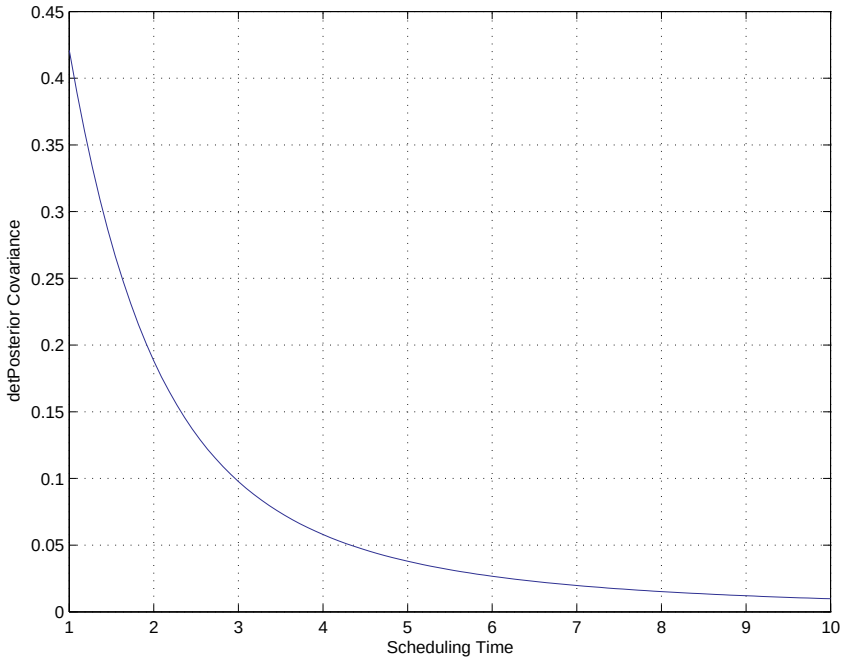

Figure 15: Determinant of State Covariance as a function of scheduling time when measurement accuracy is improved by scheduling. In this example

strictly decreasing function of time, hence is no limit on maximum allowed time for scheduling.

6.3.2 Probability of detection is improved by scheduling

In this scenario we assume R to be a constant with time and

$$p_d = 1 - \alpha/t, \qquad 0 < \alpha < 1. \tag{28}$$

We have

$$|P_{n+1|n+1}| = \det((I - p_dK)(FPF^T + Q)) = \frac{A_8(t)}{B_6(t)} \tag{29}$$

In this case $|P_{n+1|n+1}|$ behaves like $\alpha q\frac{4r_{22}+\alpha q}{12}t^2$, i.e it is increasing for large t. The function has a pole at $t = 0$ and for $t > 0$ it is positive. So that it has a local minimum for $t > 0$. The question ism does it have a local minimum at $t > 1$. This largely depends on α.

An example is shown in Figure 16. In this example $q = 1$, $R = \begin{pmatrix} 5 & 2 \\ 2 & 1 \end{pmatrix}$

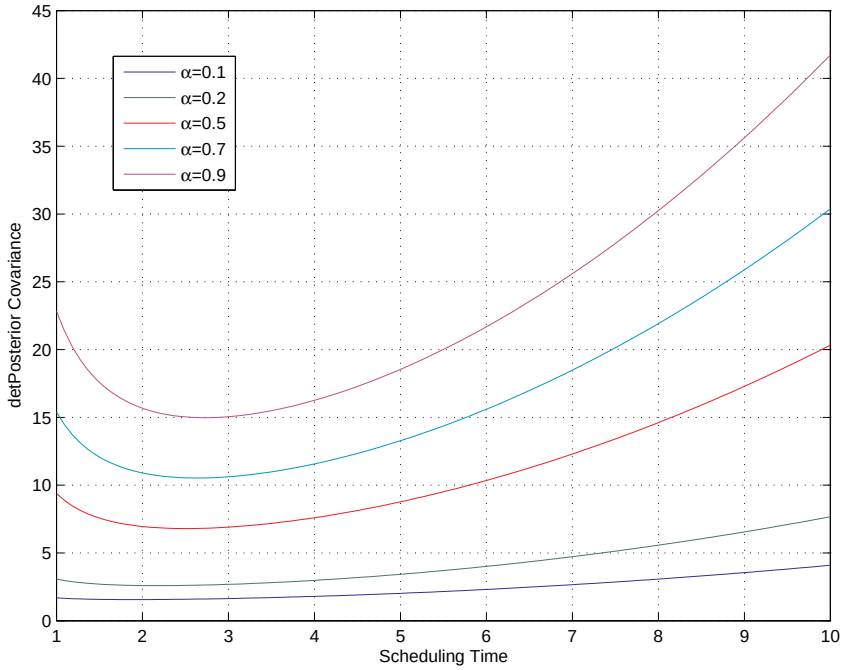

Figure 16: Determinant of State Covariance as a function of scheduling time when probability of detection is improved by scheduling.

6.3.3 Size and Shape

- Scheduling improves range measurement:

$$R = \begin{pmatrix} c_2 b^2 + c_1/t, & bc_2 \\ bc_2 & c_2 \end{pmatrix}. \tag{30}$$

- Scheduling improves Doppler measurement:

$$R = \begin{pmatrix} (c_2 b^2)/t + c_1 & (bc_2)/t \\ (bc_2)/t & c_2/t \end{pmatrix}. \tag{31}$$

  Further calculations show, that in this situation $|P_{n+1|n+1}|$ is decreasing, has no local minima in the domain, and behaves like $c_1 c_2/t$ for large t. This means that scheduling time always results in information gain. Further calculations show, that in this situation $|P_{n+1|n+1}|$ is decreasing, has no local minima in the domain, and behaves like $c_1 c_2/t$ for large t. This means that scheduling time always results in information gain.

Numerical examples are represented in Figure 17.

6.3.4 Orientation of the Measurement Noise Covariance Changes with Scheduling Time

Kalman covariance update can be re-written as

$$P_{n+1|n+1} = (P_{n+1|n}^{-1} + R^{-1})^{-1}. \tag{32}$$

Suppose it is possible to construct a waveform so that R in the form $R = AR_0A^T$, where R_0 is fixed and diagonal with the elements on the diagonal arranged is in descending order, and A is

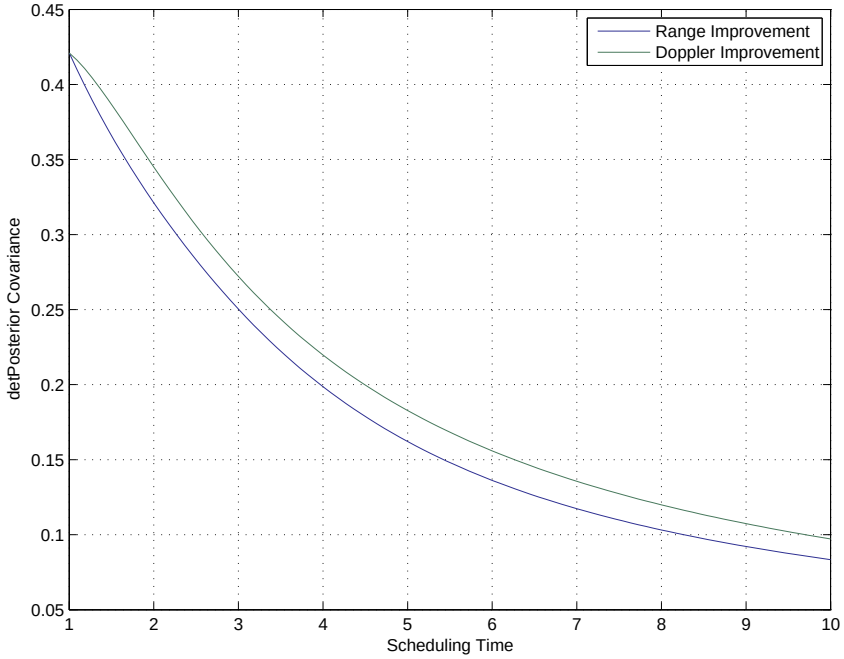

Figure 17: Determinant of State Covariance as a function of scheduling time when only range or doppler measurement is improved. In this example $q = 1$, $b = 1$, $c_1 = 1$, $c_2 = 1$

a rotation matrix with known rotation angle. Fielder [20] tells us that $|P_{n+1|n+1}|$ is maximized iff $P_{n+1|n} = AEA^T$, where E is a diagonal matrix with element on the diagonal (eigenvalues) arranged in the ascending order. In 2D this makes covariance ellipses perpendicular to each other. Lets assume that it takes time $T > 1$ to generate $R = R^\star$ perfectly perpendicular to $P_{n+1|n}$. The question is: if we use $R^\star$ at times $t < T$, do we improve the accuracy of tracking by taking a measurement at this time. Lets first look at an example. Lets say that at time $T = 10$ the ellipse of predicted covariance matrix $P_{n+1|n}$ main axis was ϕ degrees with x -axis (range), then the waveform is constructed so that its covariance matrix is

$$R = A(\phi) \begin{pmatrix} r_1 & 0 \\ 0 & r_2 \end{pmatrix} A(\phi)^{-1}, \qquad r_1 < r_2, \tag{33}$$

then $|P_{n+1|n+1}|$ is the smallest possible with respect to ϕ. Is it also the smallest with respect to t? Numerical simulations show, that the answer to the question is negative. This happens because the gain caused by orientation optimization is negligible compared to the loss caused by the growth of $P_{n+1|n}$ with time. An example is shown in Figure 18. This example suggest that measuring at time $t = 1$ is best, even though the measurement covariance matrix is "under-rotated".

6.4 Conclusion

We have investigated several situations to answer the question: how the time spent on scheduling the radar resources (to achieve better measurement) affects the accuracy of the target state. We postulated that the measurement quality improves by spending longer time at scheduling. The longer time between measurements, on the other hand, causes larger spreading in target uncertainty. We have computed the quantitative values of the parameter, for which scheduling improves target estimation and gains more information.

We also have described situations in which no improvement is possible and, in fact, in these situations scheduling will result in loss of accuracy and consequently information.

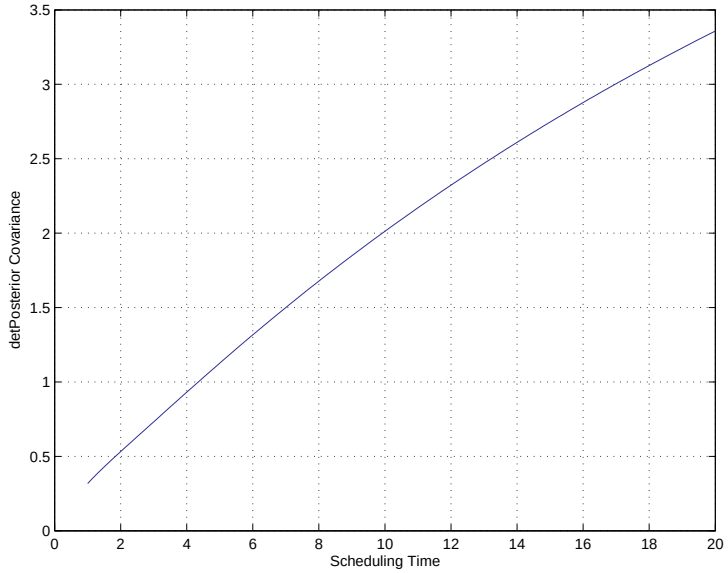

Figure 18: Determinant of State Covariance as a function of scheduling time when the orientation of the measurement covariance is improved. In this case scheduling will cause the loss of accuracy

7 More Simulation results

Recently, we have further investigated two problems, i.e., waveform scheduling and Doppler resilient Golay-type pulse trains and these works have produce close to submission papers. In addition, we also done some experimental simulations in line with the waveform scheduling.

7.1 Waveform Scheduling

Adaptive scheduling of radar and sonar sensor resources has been shown by many studies to produce significant, and some times enormous, gains in performance [21, 22]. Generally, the best performance is achieved by scheduling over an extended horizon since this allows the future consequences of current actions to be accounted for. However, finite horizon scheduling is computationally expensive and thus can rarely be used in practice. In this work we have, in collaboration with researchers at Colorado State University, specifically, Drs Ali Pezeshki and Edwin Chong and their student Zhenliang Zhang, sought ways of guaranteeing the performance of computationally efficient, but sub-optimal, greedy scheduling schemes. In particular, we have made significant advances in the area of finite horizon scheduling with string submodular objective functions. This will enable performance bounds on longer term scheduling of waveforms for radar, and, in particular, hopefully show that greedy methods for scheduling waveforms can provide close to optimal performance.

Previously we showed that for objective functions which are string submodular a greedy approach to choosing a sequence of actions achieves at least a $(1-e^{-1})$-approximation compared to the optimal approach. More recently, we have shown that these bounds can be improved by considering further properties of the objective function. In particular, if the objective function has total backward curvature σ than the performance bound for greedy scheduling becomes $(1-e^{-\sigma})/\sigma$ of the optimal strategy while for total forward curvature ϵ the bound is $(1-\epsilon)$. These results, which will appear in a forthcoming paper, more tightly bound the loss in performance for using computationally efficient greedy scheduling in place of optimal scheduling [23].

We are currently investigating the application of these general results to particular problems in radar and sonar tracking.

7.2 Doppler Resilient Golay-type Pulse Trains

Suppression of sidelobes in the ambiguity function is essential for detection of closely-separated objects in radar and sonar processing. It is well-known that complementary pulse trains are useful for sidelobe suppression. Previously, we have shown that, to achieve this suppression at non-zero Dopplers, the sequences must be sent in a particular order. With Dr Ali Pezeshki and his student Wenbing Dang, we have recently extended these results by shaping the pulse trains at both the transmit *and* receive ends. Using a receive pulse train which is not matched to the transmit pulse train allows an extra degree-of-freedom in shaping the ambiguity function, albeit with some loss in SNR.

The benefits of independently scheduling transmit and receive pulse trains are shown in Figure 19. The scene has three strong reflectors and two weak reflectors. The conventional approach, in which alternating Golay complementary waveforms are used for transmit and receive, performs poorly with the weak reflectors suppressed by the strong reflectors. Performance is significantly improved using the proposed binomial transmit-receive pulse sequence design. It can be seen that the binomial design provides sidelobe suppression for Dopplers in the range $[-1, 1]$ rad. Compared to existing techniques [24], this increases by a factor of 10 the range of sidelobe-suppressed Dopplers. As a result, weak reflectors are not masked by the strong reflectors in this example. These results are contained in the forthcoming paper [25].

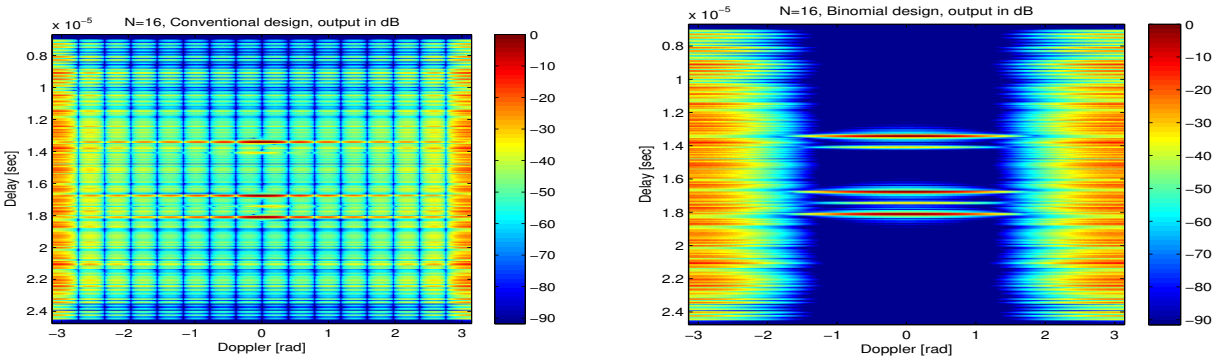

(a) Conventional (b) Binomial

Figure 19: Delay-Doppler gain using (a) conventional and (b) binomial transmit-receive design.

7.3 Complementary Pair Scheduling

Complementary waveforms achieve lowest sidelobes at zero Doppler. The idea is to schedule transmission order of waveforms to achieve optimal off-zero Doppler performance. This is achieved by using a Reed-Müller sequence tuned to Doppler region to provide transmission order. We have carried out simulations based on our recent work in [17] and results are shown in figures 20 and 21, which demonstrated that using a scheduled Reed-Müller sequence, 20dB improvement in SNR and 30% improvement in probability of detection are gained over the standard LFMs and standard complementary sequences.

7.4 Beam scheduling

We also simulated the situation of a steerable phased array radar. The aim is to selected the pointing direction so as to combine tracking and search. We use the cardinalised probability hypothesis density (CPHD) for filtering and attempt to maximise the probability of target detection. The CPHD maintains tracks as well as potential targets in unobserved areas. The detection probability is an inexpensive proxy for information gain. As shown in Fig. 22, the

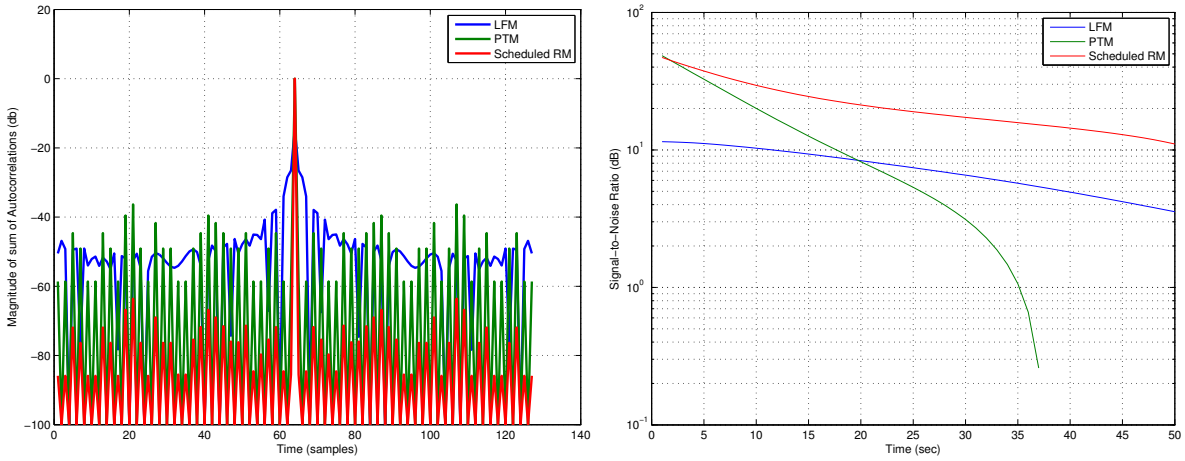

(a) (b)

Figure 20: (a) Sidelobes for standard LFMs, standard complementary, and Reed-Muller sequences. (b) SNR for standard LFMs, standard complementary, and Reed-Muller sequences.

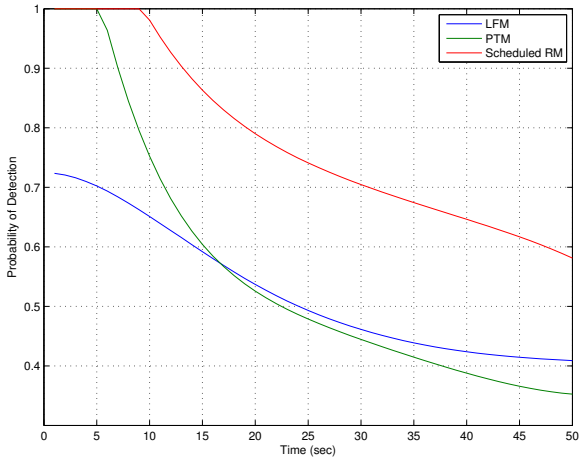

Figure 21: Detection probability for standard LFMs, standard complementary, and Reed-Muller sequences.

time required for measurement collection can be reduced by 40% by using this beam scheduling compared to regular surveillance.

7.5 LFM waveform scheduling

Another piece of work we performed is the simulation analysis of the LFM waveform scheduling. It is understand that scheduling over long horizon is computationally expensive. On the other hand, if tracking is performed with a filter of Kalman type, the long horizon scheduling is performed off-line. The objective function to be designed is such that selects waveforms from a library to maximize the information gain. Clearly, the optimisation policy depends on the dynamics of the underlying target. In the simulation, two examples of dynamics were considered: 1 — random walk with added range uncertainty (i.e sea targets), 2 — random walk. The simulation result, shown in Fig. 23, pre-computing the optimal sequence of LFM waveforms has $1/m^h$th the expense of scheduling over a horizon h with m candidate waveforms.

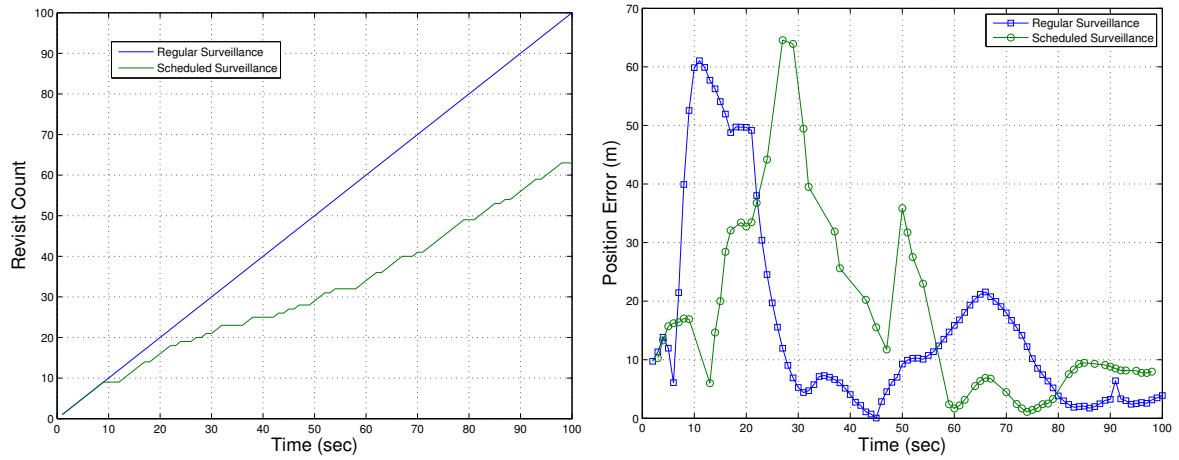

(a) (b)

Figure 22: (a) Revisit counts for for regular and schedued surveillance. (b) RMSE for regular and schedued surveillance.

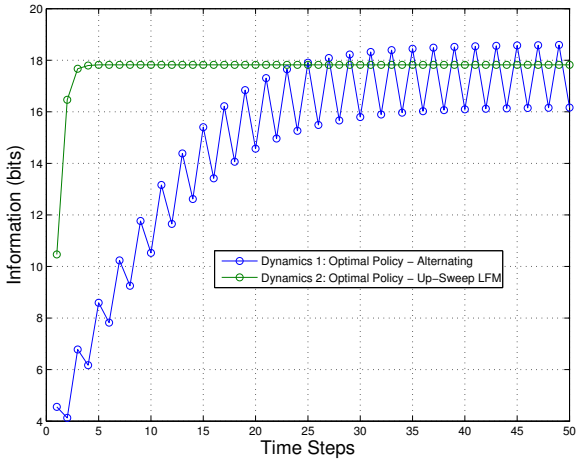

Figure 23: Optimal policies for two different process noise covariance matrices.

References

[1] T. Fortmann, Y. Bar-Shalom, M. Scheffe, and S. Gelfand, "Detection thresholds for tracking in clutter- A connection between estimation and signal processing," *IEEE Transactions on Automatic Control*, vol. 30, no. 3, pp. 221–229, 1985.

[2] M. Aslan, A. Saranli, and B. Baykal, "Tracker-aware adaptive detection: An efficient closed-form solution for the Neyman-Pearson case," *Digital Signal Processing*, vol. 20, pp. 1468–1481, 2010.

[3] S. Gelfand, T. Fortmann, and Y. Bar-Shalom, "Adaptive detection threshold optimization for tracking in clutter," *IEEE Transaction on Aerospace and Electronic Systems*, vol. 32, no. 2, pp. 514–523, 1996.

[4] Y. Bar-Shalom and E. Tse, "Tracking in a cluttered environment with probabilistic data association," *Automatica*, vol. 11, pp. 451–460, 1975.

[5] P. Willett, R. Niu, and Y. Bar-Shalom, "Integration of Bayes detection with target tracking," *IEEE Transactions on Signal Processing*, vol. 49, no. 1, pp. 17–29, 2001.

[6] F. Gini and M. Greco, "Texture modeling and validation using recorded high resolution sea clutter data," in *Proceedings of the 2001 IEEE Radar Conference, 2001*, 2001, pp. 387–392.

[7] ——, "Texture modelling, estimation and validation using measured sea clutter data," *IEE Proceedings - Radar, Sonar and Navigation*, vol. 149, no. 3, pp. 115–124, 2002.

[8] F. Gini, G. B. Giannakis, M. Greco, and G. T. Zhou, "Time-averaged subspace methods for radar clutter texture retrieval," *IEEE Transactions on Signal Processing*, vol. 49, no. 9, pp. 1886–1898, 2001.

[9] A. Farina, F. Gini, M. Greco, and L. Verrazzani, "High resolution sea clutter data: statistical analysis of recorded live data," *IEE Proceedings on Radar, Sonar and Navigation*, vol. 144, no. 3, pp. 121–130, 1997.

[10] I. Antipov, "Analysis of sea clutter data," DTIC Document, Tech. Rep., 1998. [Online]. Available: http://www.dsto.defence.gov.au/publications/1994/DSTO-TR-0647.pdf

[11] E. Conte and M. Longo, "Characterisation of radar clutter as a spherically invariant random process," *IEE Proceedings - Communications, Radar and Signal Processing*, vol. 134, no. 2, pp. 191–197, 1987.

[12] J. Li, P. Stoica, and D. Zheng, "Angle and waveform estimation in the presence of colored noise via RELAX," in *1995 Conference Record of the Twenty-Ninth Asilomar Conference on Signals, Systems and Computers, 1995*, vol. 1, 1995, pp. 433–437 vol.1.

[13] J. Li and P. Stoica, "Efficient mixed-spectrum estimation with applications to target feature extraction," *IEEE Transactions on Signal Processing*, vol. 44, no. 2, pp. 281–295, 1996.

[14] J. Li, D. Zheng, and P. Stoica, "Angle and waveform estimation via RELAX," *IEEE Transactions on Aerospace and Electronic Systems*, vol. 33, no. 3, pp. 1077–1087, 1997.

[15] "IPIX radar - dartmouth database." [Online]. Available: http://soma.ece.mcmaster.ca/ipix/dartmouth/index.html

[16] K. Ing, M. Morelande, and B. Moran., "Sea clutter modelling," *IET Radar, Sonar and Navigation*, Under Review 2015.

[17] S. Suvorova, S. Howard, and B. Moran, "Application of reed-müller coded complementary waveforms to target tracking," in *Radar (Radar), 2013 International Conference on.* IEEE, 2013, pp. 152–156.

[18] S. Suvorova, B. Moran, S. Howard, and R. Calderbank, "Application of doppler resilient complementary waveforms to target tracking," in *Acoustics, Speech and Signal Processing, 2008. ICASSP 2008. IEEE International Conference on.* IEEE, 2008, pp. 1497–1500.

[19] D. Barton and H. Ward, "Handbook of radar measurement. arthech house," 1984.

[20] M. Fiedler, "Bounds for the determinant of the sum of hermitian matrices," *Proceedings of the American Mathematical Society*, pp. 27–31, 1971.

[21] E. Chong, C. Kreucher, and A. Hero, "Partially observable markov decision process approximations for adaptive sensing," *Discrete Event Dynamic Systems*, vol. 19, no. 3, pp. 377–422, 2009.

[22] A. Hero and D. Cochran, "Sensor management: Past, present and future," *IEEE Sensors Journal*, vol. 11, no. 12, pp. 3064–3075, 2011.

[23] Z. Zhang, E. Chong, A. Pezeshki, and B. Moran, "String submodular functions with curvature constraints," *IEEE Transactions on Information Theory*, Under Review 2015.

[24] A. Pezeshki, A. Calderbank, W. Moran, and S. Howard, "Doppler resilient golay complemntary waveforms," *IEEE Transactions on Information Theory*, vol. 54, no. 9, pp. 4254–4266, 2008.

[25] W. Dang, A. Pezeshki, S. Howard, B. Moran, and R. Calderbank, "Complementary waveforms and doppler-induced sidelobes," *IEEE Transactions on Information Theory*, In preparation 2015.